



1    **Calibration and analysis of the uncertainty in downscaling global land use and**  
2    **land cover projections from GCAM**

3

4    Min Chen<sup>1\*</sup>, Chris R. Vernon<sup>2</sup>, Maoyi Huang<sup>2</sup>, Katherine V. Calvin<sup>1</sup>, and Ian P. Kraucunas<sup>2</sup>

5

6    <sup>1</sup> Joint Global Change Research Institute, Pacific Northwest National Laboratory, College Park, Maryland  
7    20740, United States

8    <sup>2</sup> Atmospheric Sciences and Global Change Division, Pacific Northwest National Laboratory, P.O. Box  
9    999, Richland, Washington 99352, United States

10

11    \*Corresponding author

12    Email: [min.chen@pnnl.gov](mailto:min.chen@pnnl.gov)

13    Telephone: 1-301-314-6755

14    Fax: 1-301-314-6719



15 **Abstract**

16 Demeter is a community spatial downscaling model that disaggregates land use and land cover  
17 changes projected by integrated human-Earth system models. Demeter has not been intensively  
18 calibrated, and we still lack a good knowledge about its sensitivity to key parameters and the parameter  
19 uncertainties. We used long-term global satellite-based land cover records to calibrate key Demeter  
20 parameters. The results identified the optimal parameter values and showed that the parameterization  
21 substantially improved the model's performance. The parameters of intensification ratio and selection  
22 threshold were the most sensitive and needed to be carefully tuned, especially for regional applications.  
23 Further, small parameter uncertainties after calibration can be inflated when propagated into future  
24 scenarios, suggesting that users should consider the parameterization equifinality to better account for the  
25 uncertainties in the Demeter downscaled products. Our study provides a key reference for Demeter users,  
26 and ultimately contribute to reducing the uncertainties in Earth system model simulations.

27

28 **Key words:** Demeter; land use and land cover change; parameterization; human-Earth systems models

29



## 30 1. Introduction

31 Land Use and Land Cover Change (LULCC) represents one of the most important human impacts on  
32 the Earth system (Hibbard et al., 2017). Besides its socioeconomic effects, LULCC is directly linked to  
33 many natural land surface processes, such as land surface energy balance, carbon and water cycle (e.g.,  
34 Piao *et al* 2007, Law *et al* 2018, Sleeter *et al* 2018, Pongratz *et al* 2006), and indirectly affects the climate  
35 system (e.g., Dickinson and Kennedy 1992, Findell *et al* 2017, Costa and Foley 2000). Thus, LULCC has  
36 been considered as a key process in simulating of Earth system dynamics, and LULCC inputs at  
37 appropriate time steps and spatial resolutions are required to match the setup of the Earth System Models  
38 (ESMs) and the nature of spatial heterogeneity of the Earth system processes (Brovkin et al., 2013;  
39 Lawrence et al., 2016; Prestele et al., 2017). While recent historical LULCC information can be obtained  
40 by ground investigation or satellite remote sensing (Friedl et al., 2002; Hansen et al., 2000; Loveland et  
41 al., 2000; Zhang et al., 2003), projections of future LULCC largely rely on mathematical models that  
42 bring socioeconomic and other diverse sectoral information together in a coherent framework to simulate  
43 the interactions between natural and human systems. However, these integrated models project LULCC at  
44 subregional level, i.e., the basic spatial units that have uniform properties for every sector (e.g.,  
45 agricultural, energy and water etc.), typically ranging from a few hundred to millions of square kilometers  
46 (Edmonds et al., 2012). For example, the GCAM model has been widely used to explore future societal  
47 and environmental scenarios under different climate mitigation policies which provides LULCC  
48 projections at region-agroecological or water basin level (Edmonds et al., 1997; Edmonds and Reilly,  
49 1985; Kim et al., 2006). ESMs divide the Earth surface into a number of grid cells and the forcing data  
50 have to be available at the same spatial resolution to drive the ESMs (Taylor et al., 2012). Therefore,  
51 spatial downscaling of the subregional LULCC becomes a critical step for linking models like GCAM  
52 and ESMs to investigate the effects of the LULCC on the processes in the natural world, and further the  
53 interactions between the human and natural systems (Hibbard and Janetos, 2013; Lawrence et al., 2012).

54 In previous studies, we have developed a land use and land cover change downscaling model, named  
55 Demeter, to bridge GCAM and ESMs (Le Page et al., 2016; Vernon et al., 2018; West et al., 2014).  
56 Demeter has been successfully applied at both global (Le Page et al., 2016) and regional (West et al.,  
57 2014) levels for downscaling GCAM-projected land use and land cover changes, and has been further  
58 developed with an extensible output module which streamlines producing specific output formats required  
59 by various ESMs (Vernon et al., 2018). However, Demeter's parameter values have been empirically  
60 determined and a complete analysis on Demeter's parametric sensitivity and uncertainties as well as a  
61 rigorous model calibration has not been conducted to help minimize the propagation of downscaling  
62 errors. The major objective of this study is to develop a framework for calibrating the key parameters of



63 Demeter, testing and quantifying the parameter sensitivities and uncertainties, and demonstrating how the  
64 parameter uncertainties would affect downscaled products.

65

## 66 **2. Method**

### 67 *2.1 Demeter*

68 Demeter is a land use and land cover change downscaling model, which is designed to disaggregate  
69 projections of land allocations generated by GCAM and other models. For example, GCAM projects land  
70 cover areas in each of its spatial units (e.g., region-agro-ecological zones, region-AEZ) for each land  
71 cover type, and Demeter uses gridded observational land cover data (e.g., satellite-based land cover  
72 product) as the reference spatial distribution of land cover types and allocates the GCAM-projected land  
73 area changes to grid level at a target spatial resolution, following some user-defined rules and spatial  
74 constraints. Below we briefly summarize the key processes of Demeter, and the detailed algorithms can  
75 be found in three earlier publications (Le Page et al., 2016; Vernon et al., 2018; West et al., 2014).

76 Demeter first reconciles the land cover classes defined in the parent model and the reference dataset  
77 to user-defined unified final land types (FLT). Downscaled land cover types will be presented in FLT.  
78 For example, if Demeter reclassifies the 22 GCAM land cover types and the 16 International Geosphere-  
79 Biosphere Programme (IGBP) land cover types from the reference dataset into 7 FLT (Forest, Shrub,  
80 Grass, Crops, Urban and Sparse), the 7 FLT will be the land types represented in Demeter's outputs by  
81 default. Demeter then harmonizes the GCAM-projected land cover areas and the reference dataset at the  
82 first time step (or 'base year') to make sure they are consistent with the GCAM spatial units and allocates  
83 the projected land cover changes by intensification and extensification. Intensification is the process of  
84 increasing a particular land cover in a grid cell where it already exists, while extensification creates new  
85 land cover in grid cells where it does not yet exist but is in proximity to an existing allocation. The order  
86 of transitions among land cover types is defined by "transition priorities" during the processes of  
87 intensification and extensification. A parameter ( $r$ , from 0 to 1) is defined as the ratio of intensification,  
88 and thus  $1-r$  of the land cover change is for extensification. Proximal relationships are defined by spatial  
89 constraints that determine the probability that a grid cell may contain a particular land use or land cover  
90 class. The current Demeter setup includes three spatial constraints: kernel density (KD), soil workability  
91 (SW) and nutrient availability (NA). For each land cover type and grid cell, KD is calculated by the  
92 spatial distance ( $D$ ) at the runtime, and SW and NA are estimated from the Harmonized World Soil  
93 Database (HWSD, FAO/IIASA/ISRIC/ISSCAS/JRC, 2012). A suitability index ( $S$ ) from 0 to 1 is defined  
94 as the weighted-average of the three spatial constraints to assess how suitable a grid cell is to receive a  
95 land cover type:

$$96 \quad S = (w_K * KD + w_S * SW + w_N * NA) / (w_K + w_S + w_N) \quad (1)$$



97 where  $w_K$ ,  $w_S$ , and  $w_N$  are the weights for KD, SW and NA, respectively, and the sum of them is 1. In the  
 98 process of extensification, Demeter ranks candidate grid cells based on their suitability indices and selects  
 99 the most suitable candidate grid cells following a user-defined threshold percentage ( $\tau$ ) for extensification.

100

101 Table 1. Transition priorities by analyzing the 24-year global land cover records from the Land Cover  
 102 CCI project of the European Space Agency Climate Change Initiative. The smaller numbers indicate  
 103 higher transition priorities.

Final Land Types (FLT <sub>s</sub> )	Final Land Types (FLT <sub>s</sub> )						
	Forest	Shrub	Grass	Crop	Urban	Snow	Sparse
Forest	0	2	3	1	4	5	6
Shrub	2	0	3	1	4	5	6
Grass	1	2	0	3	5	6	4
Crop	2	3	1	0	5	6	4
Urban	1	4	3	2	0	6	5
Snow	2	3	4	1	5	0	6
Sparse	2	3	4	1	5	6	0

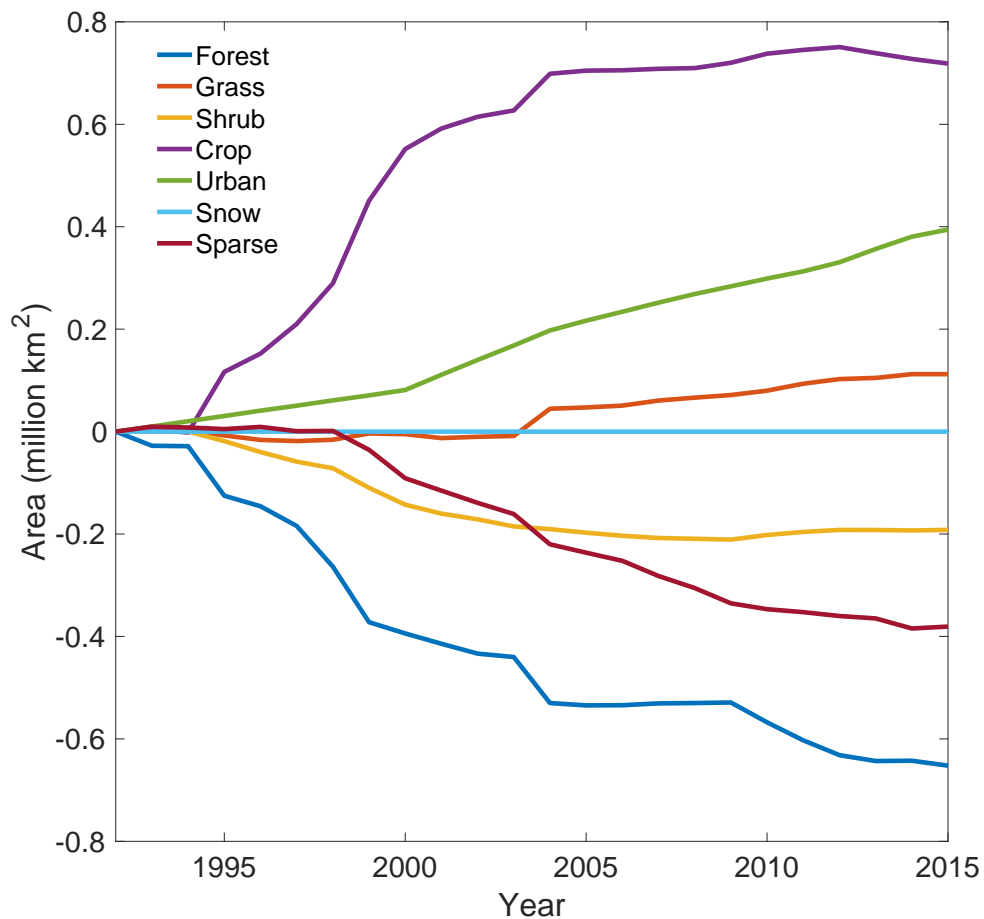
104

## 105 2.2 Calibrate Demeter with historical land cover record and sensitivity analysis

106 As indicated above, users should define a few parameters including the treatment order, the transition  
 107 priorities for allocating the land cover changes, the intensification ratio  $r$ , the selection threshold  $\tau$ , the  
 108 radius for calculating kernel density  $D$ , and weights for the spatial constraints ( $w_K$ ,  $w_S$ , and  $w_N$ ), in order to  
 109 use Demeter for downscaling projected land cover change. These parameters were determined empirically  
 110 in previous studies. Here we calibrated these parameters for Demeter using a time series of global land  
 111 cover records from the Land Cover project of the European Space Agency Climate Change Initiative  
 112 (referred to as CCI-LC products hereafter). The CCI-LC products have been generated by critically  
 113 revisiting all algorithms required for the generation of a global land cover product from various Earth  
 114 Observation (EO) instruments, thus provide a globally consistent land cover record over two decades  
 115 (1992-2015). The CCI-LC products are available at 300 m spatial-resolution and annual time step and  
 116 classify the global land cover into 38 groups. We reclassified the CCI-LC products into the default 7  
 117 FLT<sub>s</sub> (Table S1) and resampled them into 0.25° resolution with the official software tools, following the  
 118 description of CCI-LC products in the user guide  
 119 ([http://maps.elie.ucl.ac.be/CCI/viewer/download/ESACCI-LC-Ph2-PUGv2\\_2.0.pdf](http://maps.elie.ucl.ac.be/CCI/viewer/download/ESACCI-LC-Ph2-PUGv2_2.0.pdf)). Figure 1 shows  
 120 large interannual global changes for the 7 FLT areas, especially for the forests and croplands, which have



121 decreased and increased over 0.6 million km<sup>2</sup> over the past two decades, respectively. We used the  
122 gridded 0.25° CCI-LC over the 24-year period as the observational data (below referred to “LC-grid-  
123 obs”) and aggregated them into GCAM’s region-AEZ level to produce a synthetic GCAM-projected land  
124 cover change (below referred to “LC-AEZ-syn”). In this way, we can apply Demeter to LC-AEZ-syn to  
125 calibrate Demeter with the LC-grid-obs by tuning the parameters of Demeter.  
126



127  
128 Figure 1. Interannual changes of global Final Land Type (FLT) areas over 1992-2015 relative to  
129 1992, as indicated by the ESA CCI-LC product.

130 A preliminary sensitivity analysis of Demeter indicated that the downscaled results are not sensitive  
131 to treatment order and transition priorities (Le Page et al., 2016), thus we used the default treatment order,



132 i.e., from least to greatest: Urban, Snow, Sparse, Crops, Forest, Grass, Shrub. We decided the transition  
 133 priorities by sorting the probabilities of transitioning one FLT to another based on the 24-year CCI-LC  
 134 record (Table 1). To calibrate the other six parameters ( $r$ ,  $\tau$ ,  $w_K$ ,  $w_S$ ,  $w_N$  and  $D$ ), we sampled their values at  
 135 equal intervals (Table 2) and generated all possible combination (23,100 in total) for a Monte-Carlo  
 136 ensemble Demeter downscaling experiment, using LC-AEZ-syn as the input. The Monte-Carlo  
 137 experiment generated 23,100 sets of downscaled 0.25-degree global land use and land cover areas, which  
 138 were compared against LC-grid-obs to calculate their similarities to the observational data, ranked by  
 139 their discrepancies from the least to greatest to determine the likelihood of the parameters. We calculated  
 140 the discrepancies as the root mean square error ( $E_y$ ) between the downscaled and observed land cover  
 141 areas for each year:

$$E_y = \sqrt{\frac{1}{G} \frac{1}{L} \sum_g^G \sum_l^L (Ad_{y,l,g} - Ad_{o,l,g})^2} \quad (2)$$

142  
 143 and the average of the discrepancies over the years ( $E$ ):

$$E = \frac{1}{Y} \sum_y^Y E_y \quad (3)$$

144 where  $g$  is the index for  $G$  grid cells over the globe ( $G = 265,852$ ),  $l$  is the index for the  $L$  FLTs ( $L = 8$ ),  $y$   
 145 is the index for  $Y$  years. We chose 1992, 2000, 2005, 2010 and 2015 to keep consistent with the GCAM  
 146 time steps, thus  $Y = 5$ .  $Ad_{y,l,g}$  and  $Ad_{o,l,g}$  are the downscaled and observational land cover areas for grid  
 147 cell  $g$ , FLT  $l$  and year  $y$ . The unit for  $E_y$  and  $E$  is  $\text{km}^2$ .  
 148

149 To test the model sensitivity to these key parameters, we conducted a sensitivity analysis using the  
 150 results from the Monte-Carlo experiment. The first-order and total-order Sobol sensitivity indices were  
 151 used to identify the model sensitivity to each of the six parameters (Saltelli et al., 2004). Let  $X_i$  denotes  
 152 the  $i$ th parameter ( $i=1, \dots, n$ , here  $n=6$ ),  $Y$  is the model outputs (i.e.,  $E$ ), the first-order Sobol index ( $S_i$ ) is  
 153 defined as:

$$S_i = \frac{\text{Var}[E(Y | X_i)]}{\text{Var}(Y)} \quad (4)$$

154  
 155 And the total-order Sobol index ( $S_{Ti}$ ) is defined as the sum of sensitivity indices at any order  
 156 involving parameter  $X_i$ , where  $S_{ijk\dots n}$  denotes the  $n$ th-order sensitivity index:

$$S_{Ti} = S_i + \sum_{j=1, j \neq i}^n S_{ij} + \sum_{j,k=1, j,k \neq i}^n S_{ijk} + \dots + \sum_{j,k,\dots,n=1, j,k,\dots,n \neq i}^n S_{ijk\dots n} \quad (5)$$

157  
 158 The first-order Sobol index represents the contribution to the output variance of the main effect of  $X_i$ ,  
 159 therefore it measures the effect of varying  $X_i$  alone; and the total-order Sobol index measures the



160 contribution to output variance of  $X_i$  and includes all variance caused by its interactions with other  
 161 parameters. Larger Sobol indices indicate higher parameter sensitivities.

162

163 Table 2. Key parameters, and their sampling range and steps for calibration in this study.

Name	Definition	Min	Max	Sampling step
$w_N$	Weight of soil nutrient availability for calculating suitability index	0	1	0.2
$w_S$	Weight of soil workability for calculating suitability index	0	1	0.2
$w_K$	Weight of kernel density for calculating suitability index	0	1	0.2
$r$	Intensification ratio	0	1	0.1
$\tau$	Selection threshold	0	1	0.1
$D$	Kernel radius	10	100	10

164

165 *2.3 Propagate the parameter uncertainties to GCAM LULCC downscaling*

166 We selected parameter combinations which produced the smallest 5%  $E_s$  based on their rankings  
 167 from the Monte-Carlo experiment, and used them as ‘acceptable’ parameters to represent the parameter  
 168 uncertainties after calibration. We used Demeter with these parameters to downscale the GCAM-  
 169 projected LULCC at 5-year time step from 2005 to 2100 under a reference scenario to examine the  
 170 uncertainties of land cover areas for each FLT to demonstrate how different the downscaled LULCC can  
 171 be induced by the uncertain parameters. The reference scenario is a business-as-usual case with no  
 172 explicit climate mitigation efforts that reaches a higher radiative forcing level of over  $7 \text{ W m}^{-2}$  in 2100.  
 173 We only saved the downscaling results in 2005, 2010, 2050 and 2100 considering the size of the output  
 174 files and computational cost. Finally, we calculated the standard deviation across the downscaled land  
 175 cover areas for each FLT driven by different parameter combinations, which indicates the parameter-  
 176 induced model uncertainties.

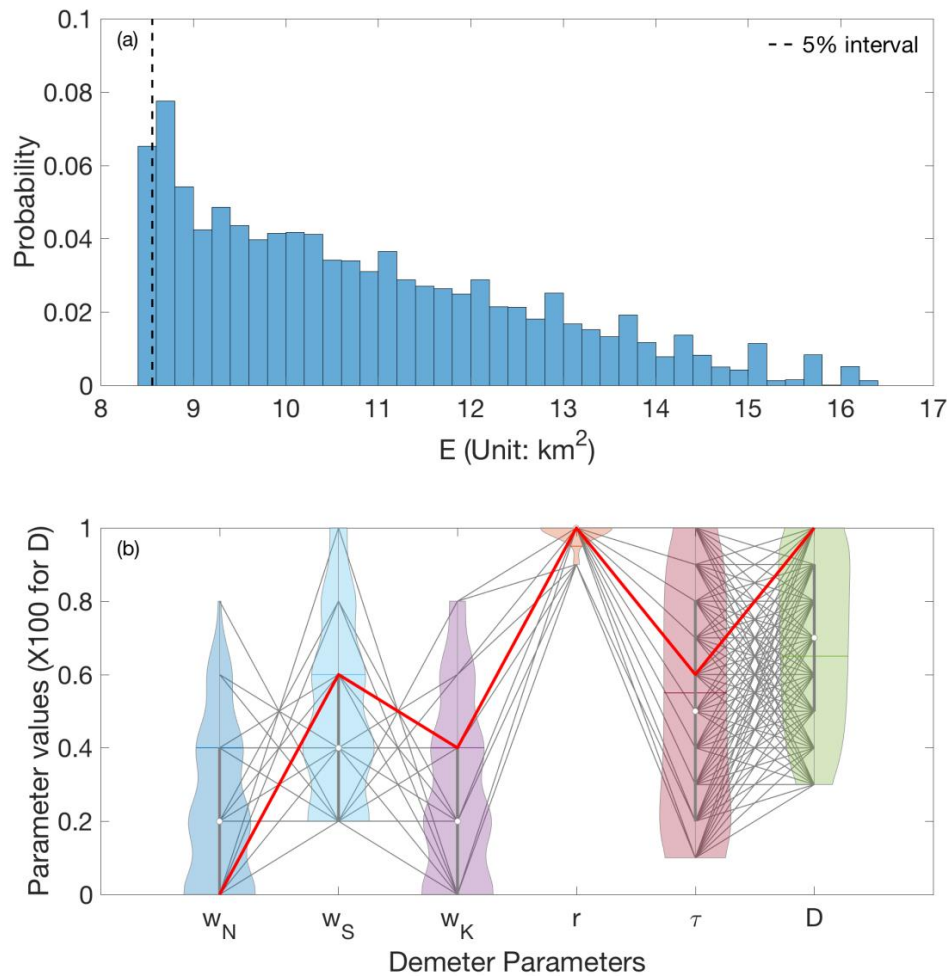
177

178 **3. Results**



179 *3.1 Parameter estimation and sensitivity*

180 The Monte-Carlo Demeter experiment driven by the 23,100 ensemble parameter sets produced  
 181 diverse downscaled LULCC realizations. As shown in Figure 2a, the disagreements between the  
 182 downscaled FLT fraction and the reference record, measured by the average root mean square error ( $E$ ,  
 183 Equation 3) for all the FLTs and grid cells over the five years (1992, 2000, 2005, 2010 and 2015), are  
 184 mainly distributed between 8 and 17 km<sup>2</sup> (about 1%-3% of the area of a 0.25-degree grid cell).

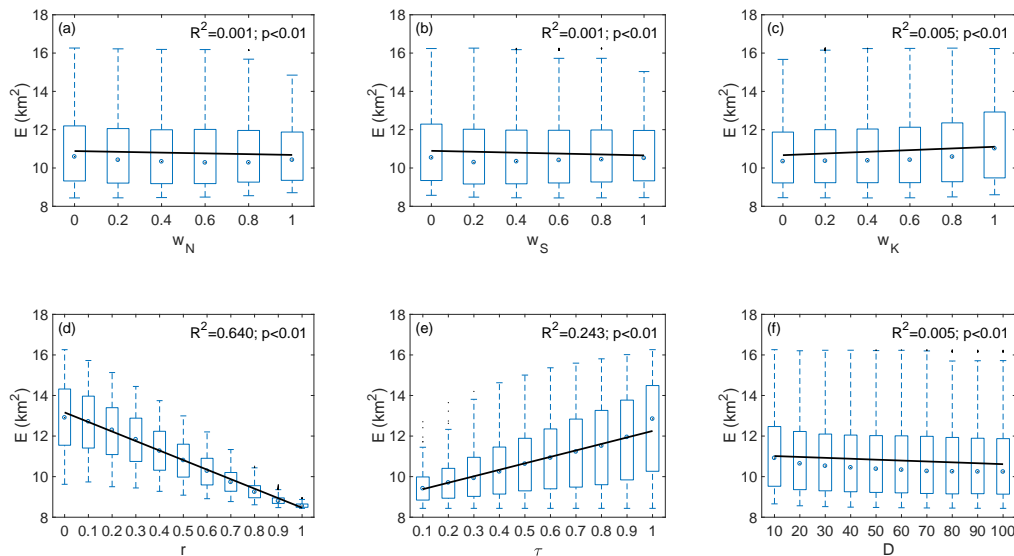


185  
 186 Figure 2. (a) Histogram of the  $E$ s, i.e., the global average discrepancies between the downscaled  
 187 and observed land cover areas with the 23,100 ensemble parameter sets; the vertical dashed line  
 188 in (a) shows the interval of the ‘best’ 5% parameters, as described in Section 2.3; (b) the  
 189 probability density of each of the ‘best’ 5% parameters, as shown by the violin plots; the black



190 lines across the six parameters show all the ‘best’ 5% parameter sets, and the red line indicates  
 191 the global optimal parameter values; the box plots and horizontal bar inside the violin plots  
 192 indicate the interquartile ranges and the mean of the parameter values, respectively. Note that the  
 193 values of  $D$  were divided by 100 for the purpose of illustration in (b).

194 Figure 3 shows the relationship between the values of the six parameters and their corresponding  $E_s$ ,  
 195 resulted from the Monte-Carlo experiment. We found that the  $E_s$  are significantly correlated to all the six  
 196 parameters ( $p < 0.01$ ). The intensification ratio ( $r$ ) has the strongest linear correlation with the  $E_s$   
 197 ( $R^2 = 0.64$ ), followed by the selection threshold ( $\tau$ ) ( $R^2 = 0.24$ ). Overall, the parameters  $w_K$  and  $\tau$  are  
 198 positively correlated with  $E_s$  (positive slopes of the trendlines), while  $w_N$ ,  $w_S$ ,  $r$  and  $D$  hold negative  
 199 correlations, indicating that smaller  $w_K$  and  $\tau$ , and larger  $w_N$ ,  $w_S$ ,  $r$  and  $D$  are associated with smaller  $E_s$ .



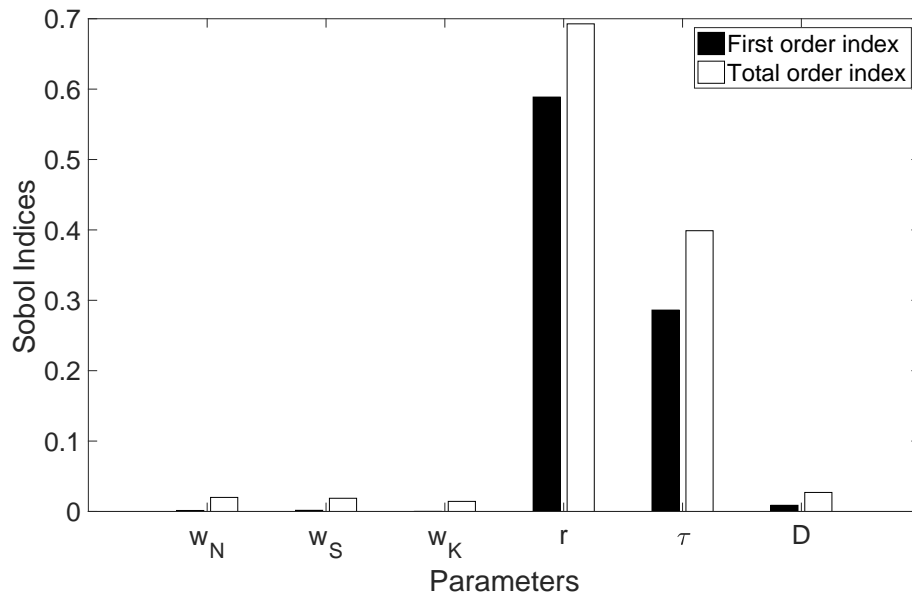
200

201 Figure 3. Relationships between the six Demeter parameters and the global average  
 202 discrepancies between the downscaled and observed land cover areas ( $E_s$ ) resulted from the  
 203 Monte-Carlo ensemble experiment. Box plots shows distributions of the  $E_s$  and the solid lines  
 204 show the linear trends.

205 Figure 4 shows the first-order and total-order Sobol indices calculated with the parameter ensemble  
 206 and the associated  $E_s$ . As indicated by the first-order Sobol indices, the intensification ratio  $r$  directly  
 207 contributes about 59% to the variability of the  $E_s$ , followed by the selection threshold  $\tau$  and kernel radius  
 208  $D$ , which directly contribute 29% and 1% to the variability of the  $E_s$ . The other parameters ( $w_N$ ,  $w_S$  and



209  $w_K$ ) have little direct contributions to the  $E$  variability. The total-order Sobol indices showed similar order  
210 of parameter importance.  $r$  and its interactions with other parameters contributed about 70% of the  $E$   
211 variability,  $\tau$  contributed about 40%,  $D$  contributed about 3%, and  $w_N$ ,  $w_S$  and  $w_K$  contributed 2%  
212 respectively. It is clear that the downscaling error is most sensitive to the intensification ratio, followed by  
213 the selection threshold, but not sensitive to the kernel radius and the weighting factors of the spatial  
214 constraints.



215

216 Figure 4. Sobol sensitivity indices for the six Demeter parameters. Higher indices indicate higher  
217 sensitivities. The first-order index measures the effect of varying a parameter alone; and the total-order  
218 index includes all variance caused by a parameter's interactions with other parameters.

219 We identified the 'best' parameters, which are associated with the lowest  $E$ , and marked them as the  
220 red line in Figure 2b. We also selected acceptable parameters that have  $E$ s lower than 5% quantile in  
221 Figure 2a and thus have the similar performance as the 'best' parameters (differences of  $E < 1\%$ ), and  
222 used them to represent the uncertainty of the parameters shown as the probability density distributions in  
223 Figure 2b. The best  $w_N$ ,  $w_S$ ,  $w_K$ ,  $r$ ,  $\tau$  and  $D$  are 0, 0.6, 0.4, 1, 0.6 and 100, respectively. All the parameters  
224 are constrained with the calibration comparing to their uniform prior distributions. The intensification  
225 ratio  $r$  has been constrained into a small range (0.9-1.0 and mostly 1.0) from 0-1.0. Constraining on the  
226 other parameters are relatively weaker:  $w_N$ ,  $w_S$ , and  $w_K$  have been narrowed to the ranges of 0-0.8, 0.2-1.0,  
227 and 0-0.8, and primarily distributed in 0-0.4, 0.2-0.6 and 0-0.4 (the first and third quantiles), respectively;

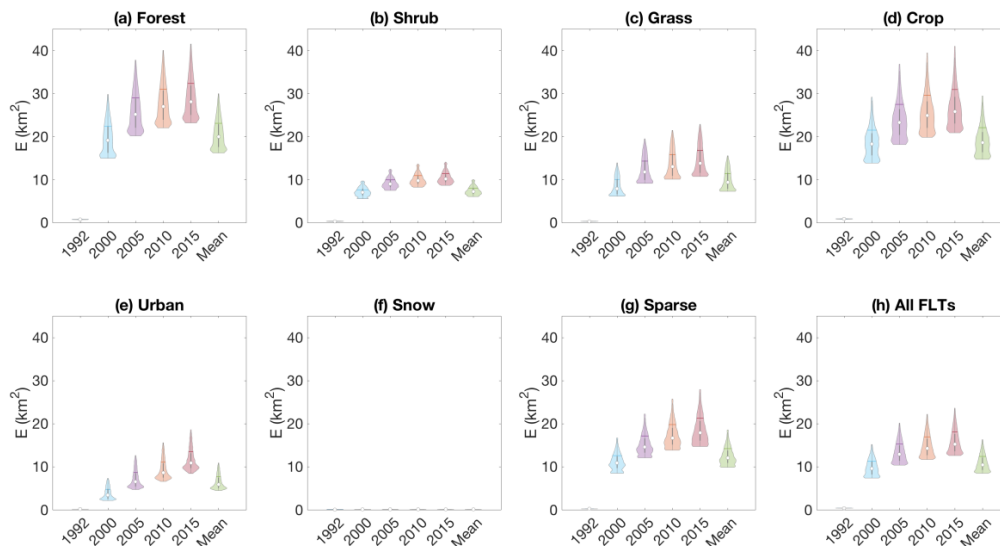


228  $\tau$  and  $D$  have been constrained into the range of 0.2-1.0 and 30-100 with the first and third quantiles being  
229 0.2-0.8 and 40-90, respectively. This analysis again indicates that  $r$  is the most sensitive parameter,  
230 therefore its posterior distribution can be significantly narrowed through the calibration.

231

### 232 3.2 Performance of Demeter in downscaling LULCC

233 Demeter generally performs well in downscaling the synthetic land use and land cover change with  
234 small disagreements with the reference data. For all FLT types, the disagreements between the downscaled  
235 FLT fraction and the reference record in 1992 (i.e.,  $E_{1992}$  in Equation 2), are close to zero since we used it  
236 as the harmonization year. The disagreements in 2000 ( $E_{2000}$ ) are mainly distributed in a range between 5  
237 and 15 km<sup>2</sup> (about 1%-2% of a 0.25-degree grid cell), with the median about 10 km<sup>2</sup> and the mean  
238 slightly above 12 km<sup>2</sup> (Figure 5h). The disagreements increase over years at a rate of about 1 km<sup>2</sup> per 5-  
239 year time step and reach 13-24 km<sup>2</sup> (median: 15 km<sup>2</sup>; mean: 18 km<sup>2</sup>) in 2015. Overall, the average  
240 disagreements over the five years ( $E$ ) mainly distributed in 8-17 km<sup>2</sup> (also shown in Figure 2a), with the  
241 median of about 10 km<sup>2</sup> and the mean of about 12 km<sup>2</sup>.



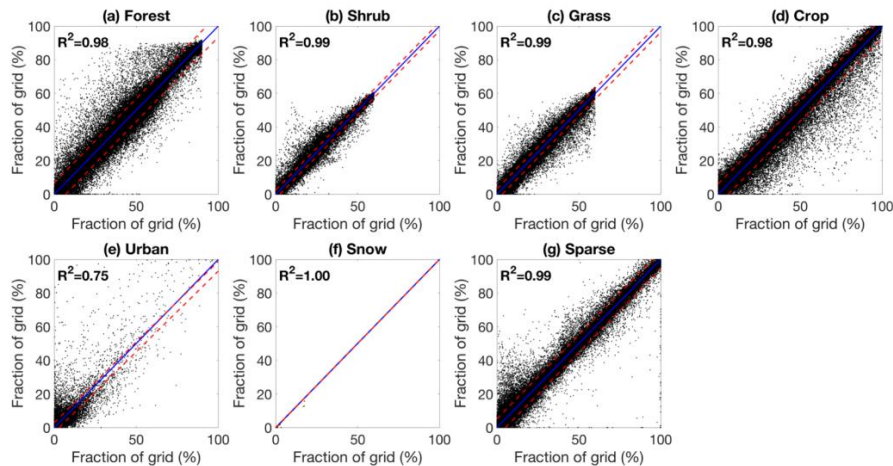
242

243 Figure 5. Possibility densities for the  $E_s$  between downscaled and observational Final Land Type  
244 areas for 1992, 2000, 2005, 2010, 2015 and the mean of the five time-steps. The box plots and  
245 horizontal bar inside the violin plots indicate the interquartile ranges and the mean of the  
246 parameter values, respectively. Note that the  $E_s$  for ‘Snow’ are close to 0 thus not visible in the  
247 figure.



248

249 The errors for each of the FLT's follow the same increasing trend over the years. Forest and crop have  
250 the largest disagreements between the downscaled and reference distributions with the errors are  
251 primarily located in the range of 20–40 km<sup>2</sup> in average over the five time steps (Figure 5a,d). The errors  
252 for sparse lands are relatively smaller, which mainly fall into the range of 10–20 km<sup>2</sup> (Figure 5g),  
253 followed by grass, shrub and urban, with the errors are mainly distributed in 0–10 km<sup>2</sup> averagely over the  
254 five years. Errors for snow is near zero since there was little areal change for this FLT in the CCI-LC  
255 record (Figure 1) and little LULCC allocation was needed in the downscaling process over the years.



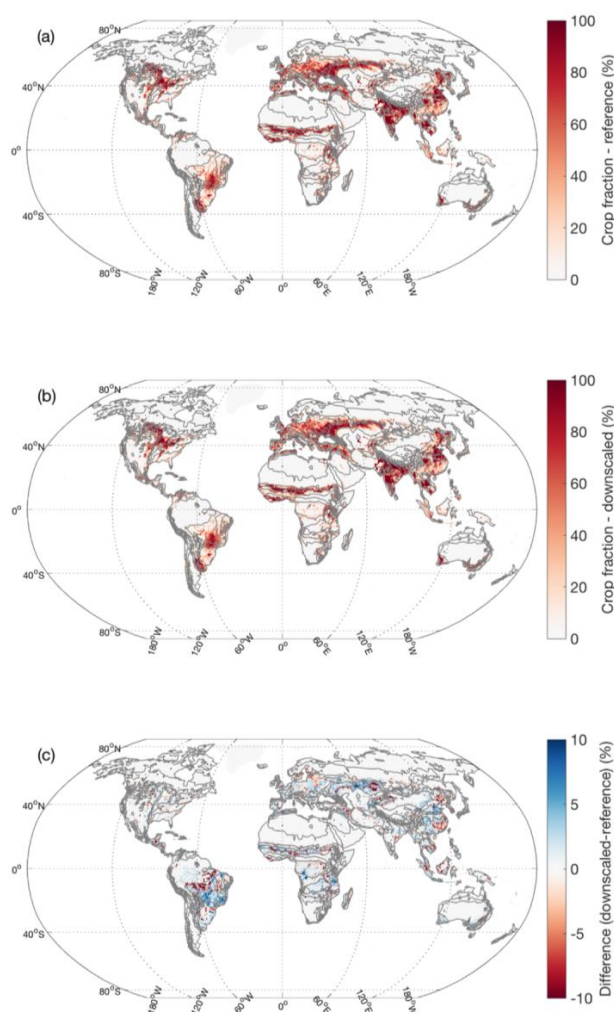
256

257 Figure 6. Comparison between the observed and downscaled Final Land Type with optimal  
258 parameters over the 265,852 0.25-degree grid cells in 2015. The blue solid lines show the 1:1 line,  
259 and the red dashed lines show the 95% confidence intervals.

260 Figure 6 shows the comparison between reference gridded CCI-LC FLT's and the downscaled FLT's  
261 driven by the best parameters (see Section 3.1) among the 265,852 0.25-degree grid cells in 2015. Except  
262 for urban, the downscaled land cover of other FLT's match the reference record very well (all R<sup>2</sup> are above  
263 0.98). The R<sup>2</sup> is 1 for snow due to little change of snow and ice area in the CCI-LC record. Figure 7  
264 demonstrates the spatial distribution of FLT fraction from the reference data and best downscaled results,  
265 together with their differences, using crop as an example. We find that the downscaled results have  
266 successfully reproduced the spatial pattern of crops from the reference data, and similar conclusions can  
267 be drawn for other FLT's (see Figure S1–S5; figure for Snow was not shown because of little change for  
268 this FLT). Misallocation of the changes primarily takes place in Brazil, China, temperate Africa and  
269 Northern Euroasia, where most of the LULCC happened over the study years.



270  
271  
272  
273  
274



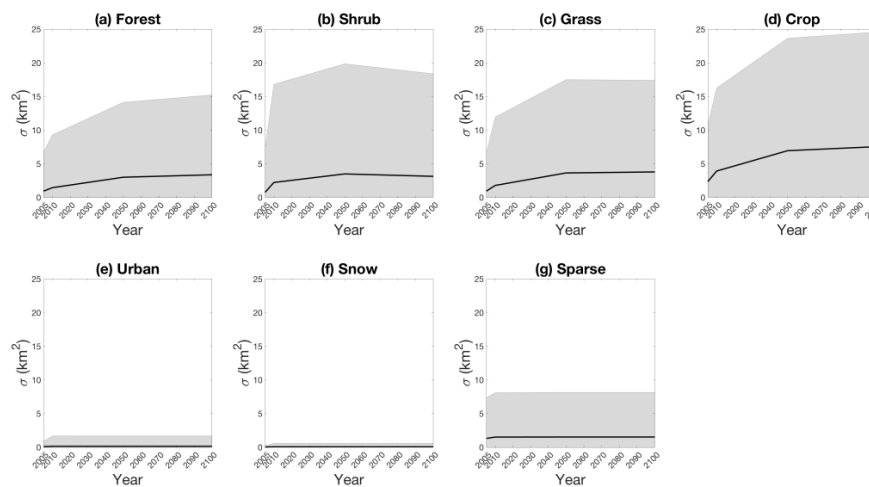
275

276 Figure 7. Spatial pattern of the observed and downscaled crop density (measured by percentage  
277 fraction of the grid cell), and their differences in 2015. The lines show the boundaries of the  
278 GCAM region-AEZs.



279 3.3 Uncertainty propagation

280 While applying the ‘acceptable’ parameters in downscaling GCAM projections of LULCC under the  
281 reference scenario, we found that these well-constrained parameters induced considerable uncertainties in  
282 the downscaled results. For each grid cell, we calculated the standard deviation ( $\sigma$ ) of the downscaled  
283 land cover areas with different parameters for each FLT (Figure S6). Figure 8 shows the mean  $\sigma$  of the  
284 265,852 0.25-degree grid cells over the globe for 2005, 2010, 2050 and 2100, as well as the spatial  
285 variability of  $\sigma$  (calculated as the standard deviation over the grid cells and shown as the shaded area in  
286 Figure 8). The uncertainty of parameters has little effect on downscaled Urban and Snow areas, since  
287 GCAM projected little areal changes of urban and snow. Downscaled sparse areas were slightly affected  
288 by the choice of parameters, indicated by small mean  $\sigma$  (about 2 km<sup>2</sup> per grid cell). However, the other  
289 FLTs, including Forest, Shrub, Grass and Crop have larger  $\sigma$ s, which also showed an increasing trend  
290 over time. The global mean  $\sigma$  for Forest, Shrub and Grass reached about 4 km<sup>2</sup> per grid cell and about 7.5  
291 km<sup>2</sup> for Crop in 2100. The spatial variability of  $\sigma$  was also larger for these FLTs, for example, the  
292 standard deviation of  $\sigma$  reached over 15 km<sup>2</sup> per grid cell in 2100 for Crop, and the maximum  $\sigma$  can be  
293 over 350 km<sup>2</sup> per grid cell in some grid cells (Figure S6).  
294



295

296 Figure 8. The mean (shown as the solid lines) and standard deviations ( $\sigma$ , shown as the shaded  
297 area) for the downscaled Final Land Type areas, when propagating the parameter uncertainties  
298 into the GCAM-projected land use and land cover change downscaling in the 21<sup>st</sup> century.



#### 299 4. Discussion

300 To date, there has been only a handful of methods for downscaling projected global land use and land  
301 cover change. For example, Oskins *et al* (2016) fitted a statistical model relating coarse-scaled spatial  
302 patterns in land cover classes to finer-scaled land cover and other explaining variables. Many more  
303 studies used complex land use modeling approach (e.g., Houet *et al* 2017, Oskins *et al* 2016, Meiyappan  
304 *et al* 2014, Hurtt *et al* 2011, Souty *et al* 2012) that combines a variety of socioeconomic processes to  
305 provide global scale land use allocations. Our results demonstrated that Demeter is an effective tool for  
306 downscaling global land use and land cover change, although it adapts a relatively simpler approach.  
307 However, choices of parameter values are critically important for a simple model, since it is possible that  
308 some complicated processes are simplified to be represented by a single parameter. Although an  
309 uncalibrated Demeter can lead to noticeable errors and uncertainties in downscaled land cover areas, our  
310 results have shown the effectiveness of the calibration efforts in minimizing the downscaling errors and  
311 constraining the uncertainties.

312 Interestingly, we found that the parameters of intensification ratio and selection threshold strongly  
313 affected the downscaled results, while the weights of the spatial constraints and kernel radius showed  
314 small impacts on the results. This result indicates that the selected spatial constraints (soil workability and  
315 nutrient availability) and spatial autocorrelation (measured by kernel density) provide loose constraints on  
316 the land allocation in the downscaling process. We also noticed that the intensification ratio has been  
317 strictly constrained to a range close to 1.0, suggesting that the intensification of land cover, especially  
318 cropland, may be the major contributor to the global land use and land cover change, thus spatial  
319 constraints on extensification are not very effective.

320 There has been a number of numerical methods for model calibration, such as gradient methods  
321 (Ypma, 1995), evolutionary algorithms (Ashlock, 2006), and data assimilation techniques (Kalnay, 2002).  
322 Our calibration method is relatively simpler, and the sampling steps are relatively coarse. As a result, it is  
323 possible that the calibrated parameters can be further improved with a more rigorous calibration strategy,  
324 although these biases should be small since the sampling bins are narrow and the sensitive parameters are  
325 well constrained (Figure 2). However, our method has a few advantages for this particular global land use  
326 and land cover change downscaling model calibration problem. First, we sampled the whole parameter  
327 space thus our Monte-Carlo downscaling experiments can well represent the parameter uncertainties.  
328 Second, the other methods mentioned above typically adjust model parameters and run the model  
329 iteratively to find the parameters to hit the local or global minimum cost function value (Chong and Zak,  
330 2013), and thus can be very time consuming due to the size of the datasets and the difficulty of algorithm  
331 parallelization. The Monte-Carlo ensemble runs of Demeter in our method can be easily parallelized and  
332 thus is computationally efficient. Finally, the saved downscaled results from the global Monte-Carlo



333 downscaling experiment can be reused for regional applications. Our study provided an optimal set of  
334 Demeter parameters. It is worth noting that these parameters are optimized to minimize the average  
335 discrepancies between the downscaled and historically observed land cover areas at the global scale, thus  
336 they may need to be recalibrated when Demeter is applied to a particular region. For example, the best  
337 estimate of the intensification ratio is 1 for a global downscaling experiment, probably due to that  
338 intensification is a more common phenomena than extensification during the past land use and land cover  
339 change in the past two decades as recorded by the ESA-CCI data. However, this high intensification ratio  
340 for Crop may be more realistic for the regions with long-term agricultural history (e.g., India), while it  
341 should become lower for the United States (US) where cropland extensification rapidly happened in the  
342 past century. We extracted the grid cells in the conterminous US (grid cells between 25° N and 50° N, and  
343 125° W and 65° W) and India (grid cells between 7° N and 33° N, and 68° E and 98° E), and used them  
344 together with the same method as the global calibration to determine the optimal parameters for the US  
345 and India, which clearly showed that the intensification ratio remained 1 for India, but moved towards  
346 lower values for the US (Figure S7).

347 Model calibration usually can provide several sets of parameters to allow the calibrated model to give  
348 similar results, which is called equifinality (Beven and Freer, 2001). As a result, the calibrated parameters  
349 become another source of uncertainty in model-simulated results. The equifinality also exists in our  
350 calibrations. We have observed noticeable growing uncertainties in downscaled land cover areas while  
351 propagating the parameter uncertainties into the Demeter downscaling practices with GCAM projected  
352 LULCC in the 21<sup>st</sup> century. Therefore, while calibration can remarkably reduce the uncertainty of the  
353 parameters, it may be better to use sets of constrained parameters rather than a single set of ‘best’  
354 parameters in the practice of Demeter, for the purpose of accounting for the parameter uncertainty and  
355 providing more reliable land use and land cover change downscaling.

356

## 357 **5. Conclusions**

358 We developed a Monte-Carlo ensemble experiment for Demeter, a land use and land cover change  
359 downscaling model of GCAM, analyzed the model’s sensitivity to its key parameters, and calibrated the  
360 parameters to minimize the mismatch between the model-downscaled and satellite-observed land use and  
361 land cover change in the past two decades. We identified the optimal parameter values for global  
362 applications of Demeter, and showed that the parameterization of Demeter substantially improved the  
363 model’s performance in downscaling global land use and land cover change. The intensification ratio and  
364 selection threshold turned out to be the most sensitive parameters, thus need to be carefully tuned,  
365 especially when Demeter is used for regional applications. Further, the small uncertainty of parameters  
366 after calibration can result in considerably larger uncertainties in the results when propagating them into



367 the practice of downscaling GCAM projections, suggesting that Demeter users consider the  
368 parameterization equifinality to better account the uncertainties in the Demeter downscaled land use and  
369 land cover changes.

370

371

#### 372 **Code Availability**

373 The source code of GCAM and Demeter is available at <https://github.com/JGCRI/gcam-core>  
374 and <https://github.com/IMMM-SFA/demeter>. The scripts for performing the calibration and analysis are  
375 available at [https://drive.google.com/open?id=1qNzh4eKgVcO\\_BjG2RjAw33whqxSMH8wm](https://drive.google.com/open?id=1qNzh4eKgVcO_BjG2RjAw33whqxSMH8wm).

376

#### 377 **Data Availability**

378 The ESA-CCI data was downloaded from <https://www.esa-landcover-cci.org/>. Other data are available at  
379 [https://drive.google.com/open?id=1qNzh4eKgVcO\\_BjG2RjAw33whqxSMH8wm](https://drive.google.com/open?id=1qNzh4eKgVcO_BjG2RjAw33whqxSMH8wm).

380

#### 381 **Author contribution**

382 M.C. conceived the study and all the authors contributed to design the study. M.C. lead the data  
383 acquisition and performed the experiment and analysis with technical assistance from C.V.; M.C. wrote  
384 the manuscript with the inputs from all the coauthors.

385

#### 386 **Competing interests**

387 The authors declare that they have no conflict of interest.

388

389

#### 390 **Acknowledgements**

391 This research was supported by the U.S. Department of Energy, Office of Science, as part of research  
392 in Multi-Sector Dynamics, Earth and Environmental System Modeling Program.

393

394

395 **References**

- 396 Ashlock, D.: Evolutionary Computation for Modeling and Optimization, Springer-Verlag, New York.,  
397 2006.
- 398 Beven, K. and Freer, J.: Equifinality, data assimilation, and uncertainty estimation in mechanistic  
399 modelling of complex environmental systems using the GLUE methodology, *J. Hydrol.*, 249(1–4), 11–29,  
400 doi:[http://dx.doi.org/10.1016/S0022-1694\(01\)00421-8](http://dx.doi.org/10.1016/S0022-1694(01)00421-8), 2001.
- 401 Brovkin, V., Boysen, L., Arora, V. K., Boisier, J. P., Cadule, P., Chini, L., Claussen, M., Friedlingstein,  
402 P., Gayler, V., van den Hurk, B. J. J. M., Hurtt, G. C., Jones, C. D., Kato, E., de Noblet-Ducoudré, N.,  
403 Pacifico, F., Pongratz, J. and Weiss, M.: Effect of Anthropogenic Land-Use and Land-Cover Changes on  
404 Climate and Land Carbon Storage in CMIP5 Projections for the Twenty-First Century, *J. Clim.*, 26(18),  
405 6859–6881, doi:10.1175/JCLI-D-12-00623.1, 2013.
- 406 Chong, E. K. P. and Zak, S. H.: An introduction to optimization, 4th Edition, John Wiley & Sons, Inc.,  
407 Hoboken, NJ., 2013.
- 408 Costa, M. H. and Foley, J. A.: Combined Effects of Deforestation and Doubled Atmospheric CO<sub>2</sub>  
409 Concentrations on the Climate of Amazonia, *J. Clim.*, 13(1), 18–34, doi:10.1175/1520-  
410 0442(2000)013<0018:CEODAD>2.0.CO;2, 2000.
- 411 Dickinson, R. E. and Kennedy, P.: Impacts on regional climate of Amazon deforestation, *Geophys. Res.*  
412 *Lett.*, 19(19), 1947–1950, doi:10.1029/92GL01905, 1992.
- 413 Edmonds, J. and Reilly, J.: *Global Energy: Assessing the Future*, Oxford University Press, New York.,  
414 1985.
- 415 Edmonds, J., Wise, M., Pitcher, H., Richels, R., Wigley, T. and Maccracken, C.: An integrated  
416 assessment of climate change and the accelerated introduction of advanced energy technologies, *Mitig.*  
417 *Adapt. Strateg. Glob. Chang.*, 1(4), 311–339, doi:10.1007/BF00464886, 1997.
- 418 Edmonds, J. A., Calvin, K. V., Clarke, L. E., Janetos, A. C., Kim, S. H., Wise, M. A. and McJeon, H. C.:  
419 Integrated Assessment Modeling, in *Encyclopedia of Sustainability Science and Technology*, edited by R.  
420 A. Meyers, pp. 5398–5428, Springer New York, New York, NY., 2012.
- 421 FAO/IIASA/ISRIC/ISSCAS/JRC: Harmonized World Soil Database (version 1.2), FAO, Rome, Italy and  
422 IIASA, Laxenburg, Austria., 2012.
- 423 Findell, K. L., Berg, A., Gentile, P., Krasting, J. P., Lintner, B. R., Malyshev, S., Santanello, J. A. and  
424 Shevliakova, E.: The impact of anthropogenic land use and land cover change on regional climate  
425 extremes, *Nat. Commun.*, 8(1), 989, doi:10.1038/s41467-017-01038-w, 2017.
- 426 Friedl, M. A., McIver, D. K., Hodges, J. C. F., Zhang, X. Y., Muchoney, D., Strahler, A. H., Woodcock,  
427 C. E., Gopal, S., Schneider, A., Cooper, A., Baccini, A., Gao, F. and Schaaf, C.: Global land cover  
428 mapping from MODIS: algorithms and early results, *Remote Sens. Environ.*, 83(1), 287–302,



- 429 doi:[https://doi.org/10.1016/S0034-4257\(02\)00078-0](https://doi.org/10.1016/S0034-4257(02)00078-0), 2002.
- 430 Hansen, M. C., Defries, R. S., Townshend, J. R. G. and Sohlberg, R.: Global land cover classification at 1  
431 km spatial resolution using a classification tree approach, *Int. J. Remote Sens.*, 21(6–7), 1331–1364,  
432 doi:[10.1080/014311600210209](https://doi.org/10.1080/014311600210209), 2000.
- 433 Hibbard, K. A. and Janetos, A. C.: The regional nature of global challenges: a need and strategy for  
434 integrated regional modeling, *Clim. Change*, 118(3), 565–577, doi:[10.1007/s10584-012-0674-3](https://doi.org/10.1007/s10584-012-0674-3), 2013.
- 435 Hibbard, K. A., Hoffman, F. M., Huntzinger, D. and West, T. O.: Changes in land cover and terrestrial  
436 biogeochemistry, in *Climate Science Special Report: Fourth National Climate Assessment, Volume I*,  
437 edited by D. J. Wuebbles, D. W. Fahey, K. A. Hibbard, D. J. Dokken, B. C. Stewart, and T. K. Maycock,  
438 pp. 277–302, U.S. Global Change Research Program, Washington, DC, USA., 2017.
- 439 Houet, T., Grémond, M., Vacquié, L., Forget, Y., Marriotti, A., Puissant, A., Bernardie, S., Thierry, Y.,  
440 Vandromme, R. and Grandjean, G.: Downscaling scenarios of future land use and land cover changes  
441 using a participatory approach: an application to mountain risk assessment in the Pyrenees (France), *Reg.*  
442 *Environ. Chang.*, 17(8), 2293–2307, doi:[10.1007/s10113-017-1171-z](https://doi.org/10.1007/s10113-017-1171-z), 2017.
- 443 Hurtt, G., Chini, L., Frolking, S., Betts, R., Feddema, J., Fischer, G., Fisk, J., Hibbard, K., Houghton, R.,  
444 Janetos, A., Jones, C., Kindermann, G., Kinoshita, T., Klein Goldewijk, K., Riahi, K., Shevliakova, E.,  
445 Smith, S., Stehfest, E., Thomson, A., Thornton, P., van Vuuren, D. and Wang, Y.: Harmonization of land-  
446 use scenarios for the period 1500–2100: 600 years of global gridded annual land-use transitions, wood  
447 harvest, and resulting secondary lands, *Clim. Change*, 109(1), 117–161, doi:[10.1007/s10584-011-0153-2](https://doi.org/10.1007/s10584-011-0153-2),  
448 2011.
- 449 Kalnay, E.: *Atmospheric modeling, data assimilation and predictability*, Cambridge University Press.,  
450 2002.
- 451 Kim, S. H., Edmonds, J., Lurz, J., Smith, S. J. and Wise, M.: The ObjECTS Framework for Integrated  
452 Assessment: Hybrid Modeling of Transportation, *Energy J.*, (Special Issue #2), 51–80, 2006.
- 453 Law, B. E., Hudiburg, T. W., Berner, L. T., Kent, J. J., Buotte, P. C. and Harmon, M. E.: Land use  
454 strategies to mitigate climate change in carbon dense temperate forests, *Proc. Natl. Acad. Sci.*, 115(14),  
455 3663 LP-3668 [online] Available from: <http://www.pnas.org/content/115/14/3663.abstract>, 2018.
- 456 Lawrence, D. M., Hurtt, G. C., Arneth, A., Brovkin, V., Calvin, K. V., Jones, A. D., Jones, C. D.,  
457 Lawrence, P. J., de Noblet-Ducoudré, N., Pongratz, J., Seneviratne, S. I. and Shevliakova, E.: The Land  
458 Use Model Intercomparison Project (LUMIP) contribution to CMIP6: rationale and experimental design,  
459 *Geosci. Model Dev.*, 9(9), 2973–2998, doi:[10.5194/gmd-9-2973-2016](https://doi.org/10.5194/gmd-9-2973-2016), 2016.
- 460 Lawrence, P. J., Feddema, J. J., Bonan, G. B., Meehl, G. A., O’Neill, B. C., Oleson, K. W., Levis, S.,  
461 Lawrence, D. M., Kluzek, E., Lindsay, K. and Thornton, P. E.: Simulating the Biogeochemical and  
462 Biogeophysical Impacts of Transient Land Cover Change and Wood Harvest in the Community Climate



- 463 System Model (CCSM4) from 1850 to 2100, *J. Clim.*, 25(9), 3071–3095, doi:10.1175/JCLI-D-11-  
464 00256.1, 2012.
- 465 Loveland, T. R., Reed, B. C., Brown, J. F., Ohlen, D. O., Zhu, Z., Yang, L. and Merchant, J. W.:  
466 Development of a global land cover characteristics database and IGBP DISCover from 1 km AVHRR  
467 data, *Int. J. Remote Sens.*, 21(6–7), 1303–1330, doi:10.1080/014311600210191, 2000.
- 468 Meiyappan, P., Dalton, M., O’Neill, B. C. and Jain, A. K.: Spatial modeling of agricultural land use  
469 change at global scale, *Ecol. Modell.*, 291, 152–174, doi:<https://doi.org/10.1016/j.ecolmodel.2014.07.027>,  
470 2014.
- 471 Oskins, A. J., Alex, B., James, G., Tom, H., N., H. L., Chris, W., J., W. K. and Simon, F.: Downscaling  
472 land-use data to provide global 30” estimates of five land-use classes, *Ecol. Evol.*, 6(9), 3040–3055,  
473 doi:10.1002/ece3.2104, 2016.
- 474 Le Page, Y., West, T. O., Link, R. and Patel, P.: Downscaling land use and land cover from the Global  
475 Change Assessment Model for coupling with Earth system models, *Geosci. Model Dev.*, 9(9), 3055–  
476 3069, doi:10.5194/gmd-9-3055-2016, 2016.
- 477 Piao, S., Friedlingstein, P., Ciais, P., de Noblet-Ducoudré, N., Labat, D. and Zaehle, S.: Changes in  
478 climate and land use have a larger direct impact than rising CO<sub>2</sub> on global river  
479 runoff trends, *Proc. Natl. Acad. Sci.*, 104(39), 15242 LP-15247 [online] Available from:  
480 <http://www.pnas.org/content/104/39/15242.abstract>, 2007.
- 481 Pongratz, J., Bounoua, L., DeFries, R. S., Morton, D. C., Anderson, L. O., Mauser, W. and Klink, C. A.:  
482 The Impact of Land Cover Change on Surface Energy and Water Balance in Mato Grosso, Brazil, *Earth  
483 Interact.*, 10(19), 1–17, doi:10.1175/EI176.1, 2006.
- 484 Prestele, R., Arneeth, A., Bondeau, A., de Noblet-Ducoudré, N., Pugh, T. A. M., Sitch, S., Stehfest, E. and  
485 Verburg, P. H.: Current challenges of implementing anthropogenic land-use and land-cover change in  
486 models contributing to climate change assessments, *Earth Syst. Dynam.*, 8(2), 369–386, doi:10.5194/esd-  
487 8-369-2017, 2017.
- 488 Saltelli, A., Tarantola, S., Campolongo, F. and Ratto, M.: Sensitivity Analysis in Practice: A Guide to  
489 Assessing Scientific Models, Wiley. [online] Available from:  
490 <http://books.google.com/books?id=NsAVmohPNpQC>, 2004.
- 491 Sleeter, B. M., Liu, J., Daniel, C., Rayfield, B., Sherba, J., Hawbaker, T. J., Zhu, Z., Selmants, P. C. and  
492 Loveland, T. R.: Effects of contemporary land-use and land-cover change on the carbon balance of  
493 terrestrial ecosystems in the United States, *Environ. Res. Lett.*, 13(4), 45006 [online] Available from:  
494 <http://stacks.iop.org/1748-9326/13/i=4/a=045006>, 2018.
- 495 Souty, F., Brunelle, T., Dumas, P., Dorin, B., Ciais, P., Crassous, R., Müller, C. and Bondeau, A.: The  
496 Nexus Land-Use model version 1.0, an approach articulating biophysical potentials and economic



497 dynamics to model competition for land-use, *Geosci. Model Dev.*, 5(5), 1297–1322, doi:10.5194/gmd-5-  
498 1297-2012, 2012.

499 Taylor, K. E., Stouffer, R. J. and Meehl, G. A.: An Overview of CMIP5 and the Experiment Design, *Bull.*  
500 *Am. Meteorol. Soc.*, 93(4), 485–498, doi:10.1175/BAMS-D-11-00094.1, 2012.

501 Vernon, C. R., Le Page, Y., Chen, M., Huang, M., Calvin, K. V., Kraucunas, I. P. and Braun, C. J.:  
502 Demeter—A Land Use and Land Cover Change Disaggregation Model, *J. Open Res. Softw.*, 6(1), 2018.

503 West, T. O., Le Page, Y., Huang, M., Wolf, J. and Thomson, A. M.: Downscaling global land cover  
504 projections from an integrated assessment model for use in regional analyses: results and evaluation for  
505 the US from 2005 to 2095, *Environ. Res. Lett.*, 9(6), 64004, 2014.

506 Ypma, T.: Historical Development of the Newton–Raphson Method, *SIAM Rev.*, 37(4), 531–551,  
507 doi:10.1137/1037125, 1995.

508 Zhang, X., Friedl, M. A., Schaaf, C. B., Strahler, A. H., Hodges, J. C. F., Gao, F., Reed, B. C. and Huete,  
509 A.: Monitoring vegetation phenology using MODIS, *Remote Sens. Environ.*, 84(3), 471–475,  
510 doi:[http://dx.doi.org/10.1016/S0034-4257\(02\)00135-9](http://dx.doi.org/10.1016/S0034-4257(02)00135-9), 2003.

511